

13th CIRP Conference on Photonic Technologies [LANE 2024], 15-19 September 2024, Fürth, Germany

# Local laser heat treatment of AlSi10Mg as-built parts produced by Laser Powder Bed Fusion

Steffen Kramer<sup>a,b,\*</sup>, Michael Jarwitz<sup>a</sup>, Volker Schulze<sup>b</sup>, Frederik Zanger<sup>b</sup>

<sup>a</sup>University of Stuttgart, Institut fuer Strahlwerkzeuge IFSW, Pfaffenwaldring 43, 70569 Stuttgart, Germany

<sup>b</sup>Karlsruhe Institute of Technology, wbk Institute of Production Science, Kaiserstraße 12, 76131 Karlsruhe, Germany

\* Corresponding author. Tel.: +49 711 685 69759; fax: +49 711 685 66842. E-mail address: [steffen.kramer@ifsw.uni-stuttgart.de](mailto:steffen.kramer@ifsw.uni-stuttgart.de)

## Abstract

Today, complex structural components for lightweight applications are frequently manufactured by laser powder bed fusion (PBF-LB), often using aluminum alloys such as AlSi10Mg. However, the application of cyclic load cases can be challenging as PBF-LB produced AlSi10Mg parts typically have low ductility and corresponding brittle failure behavior in the as-built condition.

Therefore, this paper presents investigations on the feasibility of a laser heat treatment of PBF-LB produced AlSi10Mg parts to locally increase the ductility and decrease the hardness in critical areas. Potential heat treatment process parameters were derived theoretically based on the temperature fields in the material calculated assuming three-dimensional heat conduction and a moving heat source. PBF-LB produced specimens were then laser heat treated at varying laser power and scan speed. Hardness measurements on metallographic cross sections showed hardness reductions of over 35 % without inducing hydrogen pore growth.

© 2024 The Authors. Published by Elsevier B.V.

This is an open access article under the CC BY-NC-ND license (<https://creativecommons.org/licenses/by-nc-nd/4.0>)

Peer-review under responsibility of the international review committee of the 13th CIRP Conference on Photonic Technologies [LANE 2024]

**Keywords:** laser powder bed fusion (PBF-LB); laser heat treatment; AlSi10Mg; hardness; microstructure

## 1. Introduction

Laser powder bed fusion (PBF-LB) is nowadays widely used to produce lightweight metal parts with complex geometries. One of the most common materials used in the PBF-LB process is the aluminum alloy AlSi10Mg as it is used in e.g., the aerospace or automotive sector. The material possesses a high specific strength after the PBF-LB process due to the high degree of grain refinement [1]. The application of cyclic loads however is still hindered by the typically low ductility of AlSi10Mg parts produced in PBF-LB and the scan track boundaries which promote crack propagation [1]. This results in a lower fatigue strength compared to conventional AlSi10Mg cast material [1].

It is reported that the fatigue strength of AlSi10Mg PBF-parts can be improved by different heat treatments such as the T6 heat treatment consisting of a solution annealing and a

consecutive artificial aging [2] or the direct aging process, which consists solely of an artificial aging heat treatment [3]. These heat treatments dissolve the fine microstructure and scan track boundaries and create a more homogenic structure resulting in a lower hardness and higher ductility and therefore higher fatigue strength [2] and slower crack propagation [4] but at the expense of a lower tensile strength [5]. However, these heat treatments are time and energy consuming and are always applied to the entire part, affecting areas where the high specific strength resulting of the PBF-LB process would be beneficial.

Laser heat treatment is most commonly used for laser hardening of steel materials, where rapid heating and cooling of the material surface with a defocused laser beam results in martensitic transformation, causing a local increase in hardness [6]. In [7], however, investigations are presented on a local laser heat treatment process for re-hardening the weld seam between two aluminum sheets and the heat affected zone

by introducing a precipitation hardening effect. Compared to a conventional aluminum sheet or cast material, AlSi10Mg-parts produced by the PBF-LB process already possess a high hardness but thereby also lower ductility.

Therefore, this work presents a feasibility study of a laser heat treatment process to locally adjust the microstructure for the application of cyclic loads. In a first step, an analytical model is used to estimate possible process parameters to achieve the desired temperatures and heating and cooling times. In an experimental investigation the effect of the laser heat treatment is assessed with hardness measurements and scanning electron microscope (SEM) images of the resulting microstructure.

## 2. Methods and experimental setup

For an estimation on feasible process windows, temperature distributions were calculated for three-dimensional heat conduction in a semi-infinite body and a Gaussian heat source moving at constant velocity [8]. Mirrored heat sources were implemented according to [9] to account for the finite specimen thickness. Additional mirrored heat sources were introduced to consider the finite lateral dimension. This results in a steady-state temperature field

$$\Delta T(x, y, z, s) = \frac{\eta_A \cdot P}{\pi^{3/2} \cdot \sqrt{\lambda_{th} \cdot \rho \cdot c_p}} \times \sum_{m=-\infty}^{+\infty} \sum_{n=-\infty}^{+\infty} \int_0^{\infty} \frac{\exp\left(-\frac{(x+v \cdot t)^2 + (y+m \cdot B \cdot (-1)^m)^2 + (z-2 \cdot n \cdot s)^2}{\frac{d_{spot}^2}{8} + 4 \cdot \kappa \cdot t}\right)}{\sqrt{t} \cdot \left(\frac{d_{spot}^2}{8} + 4 \cdot \kappa \cdot t\right)} dt \quad (1)$$

for a sheet material with infinite length. The following material parameters were used for the calculations: absorption coefficient  $\eta_A = 0,45$  [10], thermal conductivity  $\lambda_{th} = 115 \text{ W/(m}\cdot\text{K)}$ , density  $\rho = 2,67 \text{ g/cm}^3$  and specific heat capacity  $c_p = 900 \text{ J/(kg}\cdot\text{K)}$  [11]. Other parameters are the laser power  $P$ , the velocity ( $v$ ) of the laser beam on the specimen surface, the time  $t$ , the specimen width  $B$ , the laser spot diameter  $d_{spot} = 14 \text{ mm}$ , the thermal diffusivity  $\kappa$  and the specimen thickness  $s = 2 \text{ mm}$ . The enumerators for the mirrored heat sources are  $m$  for the lateral direction and  $n$  for the vertical direction and are set to 10 and 100, respectively.

According to [7] the hold time for a temperature above  $200 \text{ }^\circ\text{C}$  has to be between 5 to 60 seconds to enable diffusion processes in the Al-material, whereas in [11] the critical temperature for Si-diffusion in Al (Debye-temperature  $T_D$ ) is  $150 \text{ }^\circ\text{C}$ . To realize these hold times the velocity was set to  $0.8 \text{ m/min}$  and  $0.1 \text{ m/min}$  respectively and the laser power was adjusted accordingly to stay below a maximum temperature of  $500 \text{ }^\circ\text{C}$ , which is said to be the threshold temperature to induce intense hydrogen pore growth [12]. The resulting process parameters used for laser heat treatment are summarized in Table 1. Repetitive processing of the same specimen was carried out for parameter set No. 2 with a periodic duration of 90 s which assured a sufficient cooling of the sample between repetitions to avoid heat accumulation.

Table 1: Process parameter sets for laser heat treatment determined with the analytical model.

No.	Laser Power in W	Velocity in m/min	Repetitions
1	867	0.8	1
2	387	0.1	1, 3, 5 ( $\Delta t=90 \text{ s}$ )

Specimens were manufactured on a SLM 280 machine from Nikon SLM Solutions (Germany) with a laser power of  $350 \text{ W}$ , scanning speed of  $1150 \text{ mm/s}$ , hatch distance of  $170 \text{ }\mu\text{m}$ , layer thickness of  $50 \text{ }\mu\text{m}$  and a focus diameter of  $83 \text{ }\mu\text{m}$ . The process parameters were provided by the system manufacturer and are targeted for maximum part density in industrial applications. AlSi10Mg powder material with a powder size distribution of  $20\text{--}63 \text{ }\mu\text{m}$  was supplied by m4p material solutions (Austria). Rectangular sheets with a size of  $30 \times 50 \text{ mm}^2$  and a thickness of  $2 \text{ mm}$  were manufactured in an upright orientation and with a base plate temperature of  $100 \text{ }^\circ\text{C}$ . Specimens were cleaned and cut from the base plate using wire EDM.

Laser heat treatment was carried out on the sheet surface along the build direction with a defocused laser beam from a TruDisk 16002 disk laser (TRUMPF, Germany) with a wavelength of  $1030 \text{ nm}$  ( $M^2 \sim 23$ ) resulting in a laser spot diameter of  $14 \text{ mm}$  on the specimen surface and a near-gaussian intensity distribution in the far field. To minimize the heat loss, specimens were isolated with rough sandpaper, which guaranteed for minimal contact with the clamping. The experimental setup is schematically depicted in Fig. 1.

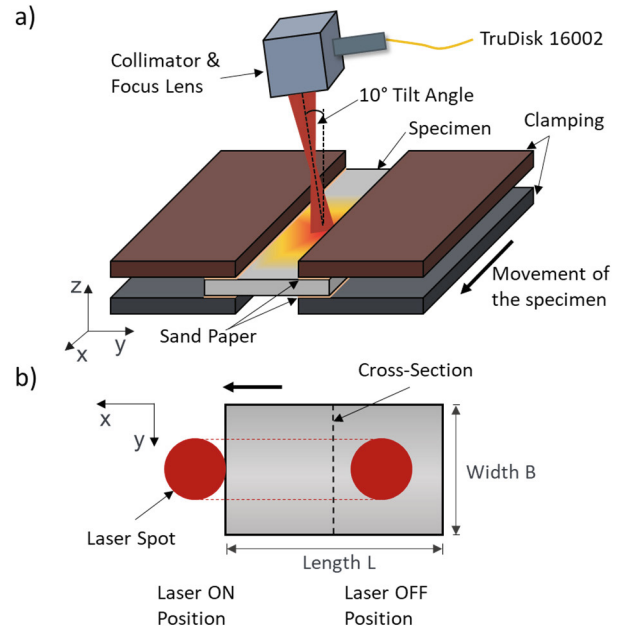


Fig. 1: a) Schematic experimental setup of the laser heat treatment; b) Scaled presentation of the laser beam and movement on the sheet sample ( $s = 2 \text{ mm}$ ).

For every parameter set two specimens were subjected to the laser heat treatment and subsequently cut in the middle, embedded, grinded and polished. Vickers hardness was measured along the cross-section with an ATM Carat 930 (ATM, Germany) hardness tester and a testing force of  $0.98 \text{ N}$ . For every specimen at least three hardness profiles were measured. Cross-sections were electro-chemically etched using Barker's reagent. Microstructure investigations were carried out with a JSM-6490LV SEM (Jeol, Japan).

### 3. Results

In Fig. 2 the temperature curves for the determined process parameters are depicted, illustrating the different hold times and maximum temperatures. With a laser power of 387 W and a velocity of 0.1 m/min the calculated maximum temperature is approx. 464 °C and the temperature stayed above 150 °C for 54 s. The higher laser power (867 W) and higher velocity (0.8 m/min) lead to a similar calculated maximum temperature of 488 °C and a shorter hold time of 4.5 s. These results are in good agreement with the boundary conditions presented in the literature above.

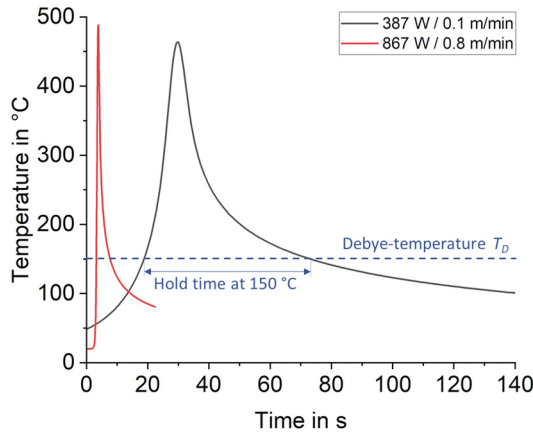


Fig. 2: Analytically calculated temperature curves for different process parameters, assuming a stationary process and a sheet material with infinite length. The hold time for parameter set 2 at 150 °C is highlighted.

For every parameter set all measured hardness profiles were averaged and the standard deviation (SD) was calculated. The resulting hardness profiles are shown in Fig. 3.

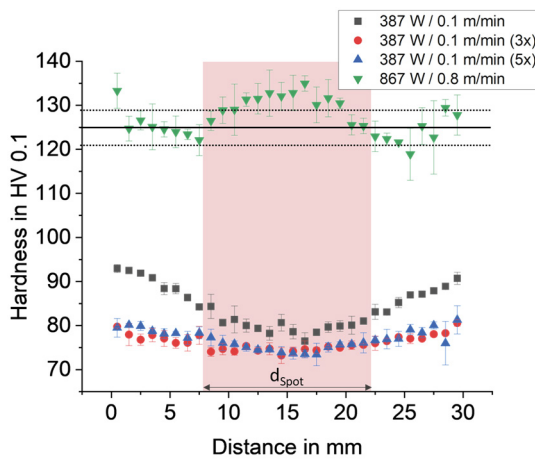


Fig. 3: Hardness measurements along the cross-sections for different laser heat treatment parameters. The horizontal lines indicate the initial hardness and standard deviation (dashed lines).

The initial hardness of an as built specimen was measured with 124.7 HV (SD=4.1). Laser heat treatment with parameter set 1 results in a slight hardness increase only in the area covered by the laser spot. In the middle of the laser spot the hardness reached a maximum value of 135 HV. Next to the laser spot the measured hardness matches the initial values. The hardness profile of the second parameter set exhibits a

significant overall reduction with a minimum hardness value of 76.5 HV in the middle of the laser spot and 93 HV at the rim of the specimen. Repetitions of the heat treatment result in a homogeneous hardness along the cross-section with no local hardness deviations.

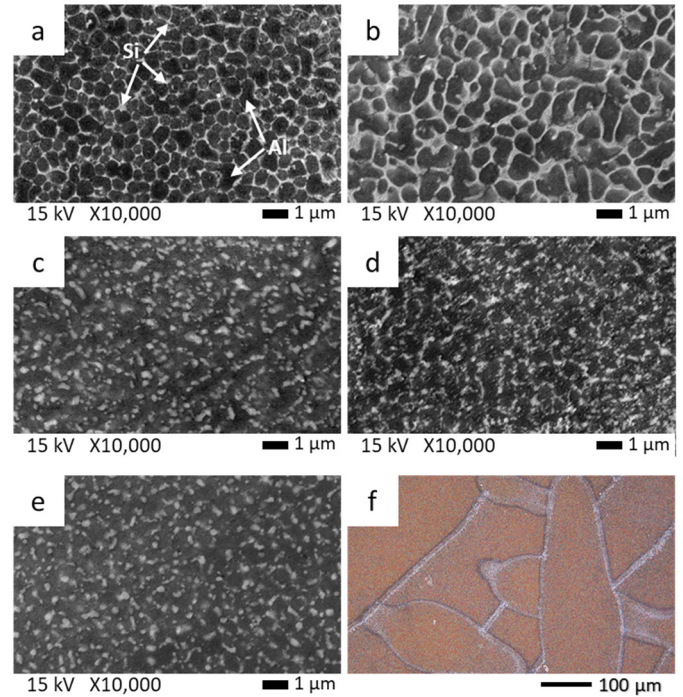


Fig. 4: SEM and OM images of the microstructure: a) as built, b) 867 W / 0.8 m/min, c) 387 W / 0.1 m/min (center), d) 387 W / 0.1 m/min (rim), e) 387 W / 0.1 m/min – 5 repetitions, f) OM image of the melt tracks for 387 W / 0.1 m/min – 5 repetitions.

SEM and optical microscope (OM) images of the resulting microstructure are shown in Fig. 4. To avoid heat-affected zones at the scan track boundaries and to ensure comparable microstructures, all SEM images were taken from the center of the scan tracks and all images except Fig. 4d were taken from the center of the specimen at  $y=15$  mm. The microstructure of the as-built specimen consists of an intact, cellular Si-rich network (see Fig. 4a, light gray structure). After laser heat treatment with 867 W and 0.8 m/min (parameter set 1) the network appears thicker and the cellular structure is damaged at multiple positions (Fig. 4b).

Heat treatment with parameter set 2 leads to an almost complete break-up of the network structure in the center of the specimen (Fig. 4c). At the rim of the specimen (Fig. 4d) the cellular structure can still be identified as the Si-particles are smaller compared to the center and map the position of the dissolved Si-network. Measurements showed that at the rim Si-particles are in average around 100 nm in diameter whereas in the center the average diameter is around 170 nm. Repeating the heat treatment with parameter set 2 does not significantly change the microstructure (Fig. 4e). No increased porosity was found in the OM images and all specimens (incl. as-built) showed the same relative density of around 99.5 % measured by image evaluation, indicating that the applied temperature profiles did not initiate the growth of hydrogen pores.

## 4. Discussion

The cellular microstructure in the as-built specimen (compare Fig. 4a) consists of a Si-rich network and an  $\alpha$ -Al Matrix supersaturated with Si [5, 13]. The high cooling rate of the PBF-process inhibits extensive diffusion of Si-atoms and enhances the solubility of Si in Al [5, 13]. The resulting fine grains contribute to an extensive increase in hardness [13] and tensile strength compared to cast material [5].

Near the rim of the specimen the network structure is broken and Si agglomerates in near-spherical shape along the former network structures (see Fig. 4d). This is presumably caused by elevating the temperature above  $T_D$  during laser heat treatment and thereby enable Si-diffusion. In the center Si-particles are larger and distributed more homogeneous as the Si-agglomeration has progressed further (Fig. 4c & e). This can be explained by the higher maximum temperature and hold time in the center of the specimen due to the direct illumination by the laser beam.

In the following the results of the present investigation are compared to published results of global heat treatment processes: A similar microstructure as in Fig 4c was achieved by [14] with conventional, global heat treatment at 290 °C but with a 60-times longer duration of around 50 min. The measured hardness however is in good agreement with the values measured in the present study for parameter set 2 in the center of the specimen. In [15] it is reported, that a salt bath heat treatment of AlSi10Mg as-built samples for only 60 s at a temperature of 300 °C was sufficient to initiate the break-up of the Si-network and lower the hardness to 105 HV. According to the calculated temperature curve for parameter set 2 in Fig. 2 the center of the specimen presumably experienced temperatures higher than 300 °C for around eleven seconds but achieved a much lower hardness of 76.5 HV. In terms of microstructure, it therefore appears possible to compensate for and exceed the shorter hold time with higher temperatures. The short process time may also explain why the laser heat treatment, compared to a conventional heat treatment, was not able to dissolve the scan track boundaries, as shown in Fig. 4f.

In [13] it is reported that with a global low-temperature annealing of 180 °C for 30 min it is possible to even increase the hardness of as-built specimens from 125 to 140 HV. This hardness increase is led back to the formation of needle-like Si-precipitations in the supersaturated  $\alpha$ -Al. After 30 minutes over-aging begins and the Si-network slowly dissolves, causing the hardness to drop again. Although it was not possible to confirm the formation of these needle-like precipitations, this effect could be a possible explanation for the slight increase in hardness in the center of the specimen for parameter set 1.

## 5. Conclusion

The present work proves the feasibility of microstructure adjustments with a local laser heat treatment of AlSi10Mg-parts produced by powder bed fusion. An analytical model was used to derive promising process parameters for the laser heat treatment. Experimental investigations have shown that with a calculated hold time of about 54 s above  $T_D$ , it is possible to reduce hardness by around 35 %, while short hold times of

about 5 s led to a slight, local increase in hardness. Lower hardness values are attributed to a dissolution of the Si-rich network and the formation of spherical Si-grains. Hardness gain could be caused by needle-shaped Si-precipitations. Further research is needed to restrict the observed heat treatment effect to smaller areas, e.g. by using smaller laser spot sizes, and to assess the impact on fatigue performance.

## Acknowledgements

The presented work was funded by the Ministry of Science, Research and the Arts of the Federal State of Baden-Wuerttemberg within the ‘InnovationCampus Future Mobility’, which is gratefully acknowledged. The authors declare no conflict of interests in this work.

## References

- [1] Yan Q, Song B, Shi Y. Comparative study of performance comparison of AlSi10Mg alloy prepared by selective laser melting and casting. *J Mater Sci Technol.* 2020;41:199-208.
- [2] Brandl E, Heckenberger U, Holzinger V, Buchbinder D. Additive manufactured AlSi10Mg samples using Selective Laser Melting (SLM): Microstructure, high cycle fatigue, and fracture behavior. *Mater. Des.* 2012;34:159-169.
- [3] Egidio GD, Ceschini L, Morri A, Zanni M. Room- and High-Temperature Fatigue Strength of the T5 and Rapid T6 Heat-Treated AlSi10Mg Alloy Produced by Laser-Based Powder Bed Fusion. *Metals* 2023;13:263.
- [4] Santos Macias JG, Elangeswaran C, Zhao L, Buffière JY, Van Hooreweder B, Simar A. Fatigue crack nucleation and growth in laser powder bed fusion AlSi10Mg under as built and post-treated conditions. *Mater. Des.* 2021;210:110084.
- [5] Van Cauwenbergh P, Samaee V, Thijs L, Nejezhlebová J, Sedláč P, Ivekovic A, Schryvers D, Van Hooreweder B, Vanmeensel K. Unravelling the multi-scale structure–property relationship of laser powder bed fusion processed and heat-treated AlSi10Mg. *Sci Rep* 2021;11:6423
- [6] Moradi M, Arabi H, Nasab SJ, Benyounis KY. A comparative study of laser surface hardening of AISI 410 and 420 martensitic stainless steels by using diode laser. *Opt. Laser Technol* 2019;111:347-357.
- [7] Faure F, Hagenlocher C, Leis A, Weber R, Graf T, Bassi C. Local Hardness recovery in the heat affected zone of laser beam weld seams in AlMgSi-alloys with an in-process laser post-heat treatment. *ICALEO 2021, Laser Institute of America*, October 2021
- [8] Cline HE, Anthony TR. Heat treating and melting material with a scanning laser or electron beam. *J. Appl. Phys* 1977;48:3895.
- [9] Jarwitz M, Weber R, Graf T. Analytical model for the extent of the heat-affected zone occurring during overlap laser welding of dissimilar materials. *J. Appl. Phys* 2017;122:135104
- [10] Leis A, Weber R, Graf T. Influence of the process parameters on the absorptance during Laser-Based Powder Bed Fusion of AlSi10Mg. *Proc CIRP* 2020;94:173-176
- [11] Yang P, Deibler LA, Bradley DR, Stefan DK, Carroll JD. Microstructure evolution and thermal properties of an additively manufactured, solution treatable AlSi10Mg part. *J. Mater. Res.* 2018;33:No23
- [12] Strumza E, Hayun S, Barzilai S, Finkelstein Y, David RB, Yeheskel O. In situ detection of thermally induced porosity in additively manufactured and sintered objects. *J Mater Sci* 2019;54:8665-8674
- [13] Fousová M, Dvorský D, Michalcová A, Vojtech D. Changes in the microstructure and mechanical properties of additively manufactured AlSi10Mg alloy after exposure to elevated temperatures. *Mater Charact* 2018; 137:119-126.
- [14] Fiocchi J, Tuissi A, Biffi CA. Heat treatment of aluminium alloys produced by laser powder bed fusion: A review. *Mater. Des.* 2021;204:109651
- [15] Takata N, Liu M, Kodaira H, Suzuki A, Makoto K. Anomalous strengthening by supersaturated solid solutions of selectively laser melted Al–Si-based alloys. *Addit. Manuf* 2020;33:10115.